BAMS Article

Aviation Impacts on Fuel Efficiency of a Future More Viscous Atmosphere

Diandong Ren, Rong Fu, Robert E. Dickinson,
Lance M. Leslie, and Xingbao Wang

Downloaded from http://journals.ametsoc.org/bams/article-pdf/101/10/E1761/5013924/bamsd190239.pdf by guest on 24 November 2020

ABSTRACT: Aircraft cruising near the tropopause currently benefit from the highest thermal efficiency and the least viscous (sticky) air, within the lowest 50 km of Earth's atmosphere. Both advantages wane in a warming climate, because atmospheric dynamic viscosity increases with temperature, in synergy with the simultaneous engine efficiency reduction. Here, skin friction drag, the dominant term for extra aviation fuel consumption in a future warming climate, is quantified by 34 climate models under a strong emissions scenario. Since 1950, the viscosity increase at cruising altitudes (~200 hPa) reaches ~1.5% century^{-1}, corresponding to a total drag increment of ~0.22% century^{-1} for commercial aircraft. Meridional gradients and regional disparities exist, with low to midlatitudes experiencing greater increases in skin friction drag. The North Atlantic corridor (NAC) is moderately affected, but its high traffic volume generates additional fuel cost of ~3.8×10^7 gallons annually by 2100, compared to 2010. Globally, a normal year after 2100 would consume an extra ~4×10^6 barrels per year. Intermodel spread is <5% of the ensemble mean, due to high inter–climate model consensus for warming trends at cruising altitudes in the tropics and subtropics. Because temperature is a well-simulated parameter in the IPCC archive, with only a moderate intermodel spread, the conclusions drawn here are statistically robust. Notably, additional fuel costs are likely from the increased vertical shear and related turbulence at NAC cruising altitudes. Increased flight log availability is required to confirm this apparent increasing turbulence trend.

https://doi.org/10.1175/BAMS-D-19-0239.1
Corresponding author: Dr. Diandong Ren, diandong.ren@curtin.edu.au, rendianyun@gmail.com; Lance M. Leslie, Lance.Leslie@uts.edu.au
Supplemental material: https://doi.org/10.1175/BAMS-D-19-0239.2

In final form 15 May 2020
©2020 American Meteorological Society
For information regarding reuse of this content and general copyright information, consult the AMS Copyright Policy.

AFFILIATIONS: Ren—School of Electrical Engineering, Computing and Mathematical Sciences, Curtin University, Perth, Western Australia, Australia; **Fu and Dickinson**—Department of Mathematical Science, University of California, Los Angeles, Los Angeles, California; **Leslie**—University of Technology Sydney, Sydney, New South Wales, Australia; **Wang**—College of Oceanography, Hohai University, Nanjing, China

Aviation is an important and rapidly growing industry sector that has long been recognized as sensitive to environmental changes (Zillman 1997; Lee et al. 2009; ICAO 2014; Ren et al. 2018) and also contributes to many aspects of atmospheric composition and radiative balance [e.g., the 1999 Intergovernmental Panel on Climate Change (IPCC) Special Report on Aviation and Global Atmosphere and references therein; Heymsfield et al. 2010, 2017; Lee and Fahey 2016]. Over the past 100 years, aircraft have become an indispensable means of transportation that physically connects the world's cities (Fig. 1a). The frequency and density of air traffic often is an indicator of socioeconomic well-being. For example, China presently possesses the most frequent commercial flights and contributes the largest share of the global air traffic expansion. The large coverage of flight tracks over the globe (especially oceanic areas; Fig. 1b) makes the aircraft measurements an important data source to initialize weather prediction models. Technically, airplane design is approaching the limit for breathing thermal engines, which intake ambient air. Currently, under the dual requirements of safety and efficiency of expanding worldwide air traffic, with projected doubling of the 2010 level by ~2030 (e.g., ICAO 2014), perfecting electrification and achieving various environmental objectives have become major goals of the aviation industry. For the same transportation capacity, fuel efficiency also is directly proportional to emissions and thereby to the environmental footprint size of an aircraft. Given rising greenhouse gas concentrations and the vast size of the aviation industry, the chain of events could already be underway. Accordingly, fuel efficiency, along with improved safety, occupies a central position in the future civil aviation industry.

Aside from passenger comfort and safety, of most concern to the aviation industry with a warming climate may likely be the following two questions, relevant for both passenger and cargo aircraft: 1) How is the maximum payload affected by the warmer and lighter lower atmosphere; and 2) during the journey, will the changed ambient air properties (density, temperature, and viscosity) involve more fuel consumption, either through affecting the engine performance, or because extra work needs to be done? The first question largely is a transportation capacity issue. The first-order response to a warming climate is the expanded volume of Earth's atmosphere and hence a reduced lower-level density. Hence there is a high consensus that payloads will be reduced in a warming future climate (e.g., Coffel and Horton 2015; Ren et al. 2018; Gratton et al. 2020). The second question, which principally is a fuel efficiency issue, is more complex. Any factors directly invoking extra work done during flight, or affecting the engine performance, are relevant to fuel efficiency. Notably, there are many canceling effects. For example, temperature affects thermal efficiency and mechanical efficiency oppositely (Ren and Leslie 2019a). Similarly, varying velocity–density pairs that satisfy the same payload requirement has an ambiguous net effect on total resistance. For example, resistance is proportional to density, suggesting that aircraft should fly higher, in a less dense layer for fuel efficiency. However, aside from the extra potential energy needed to climb to a higher cruising altitude, supporting the same payload in a reduced density environment involves a proportionally increased cruising speed. Because resistance is proportional to the square of velocity, it is not easy to decide whether reduced density or

Downloaded from http://journals.ametsoc.org/bams/article-pdf/101/10/E1761/5013924/bamsd190239.pdf by guest on 24 November 2020

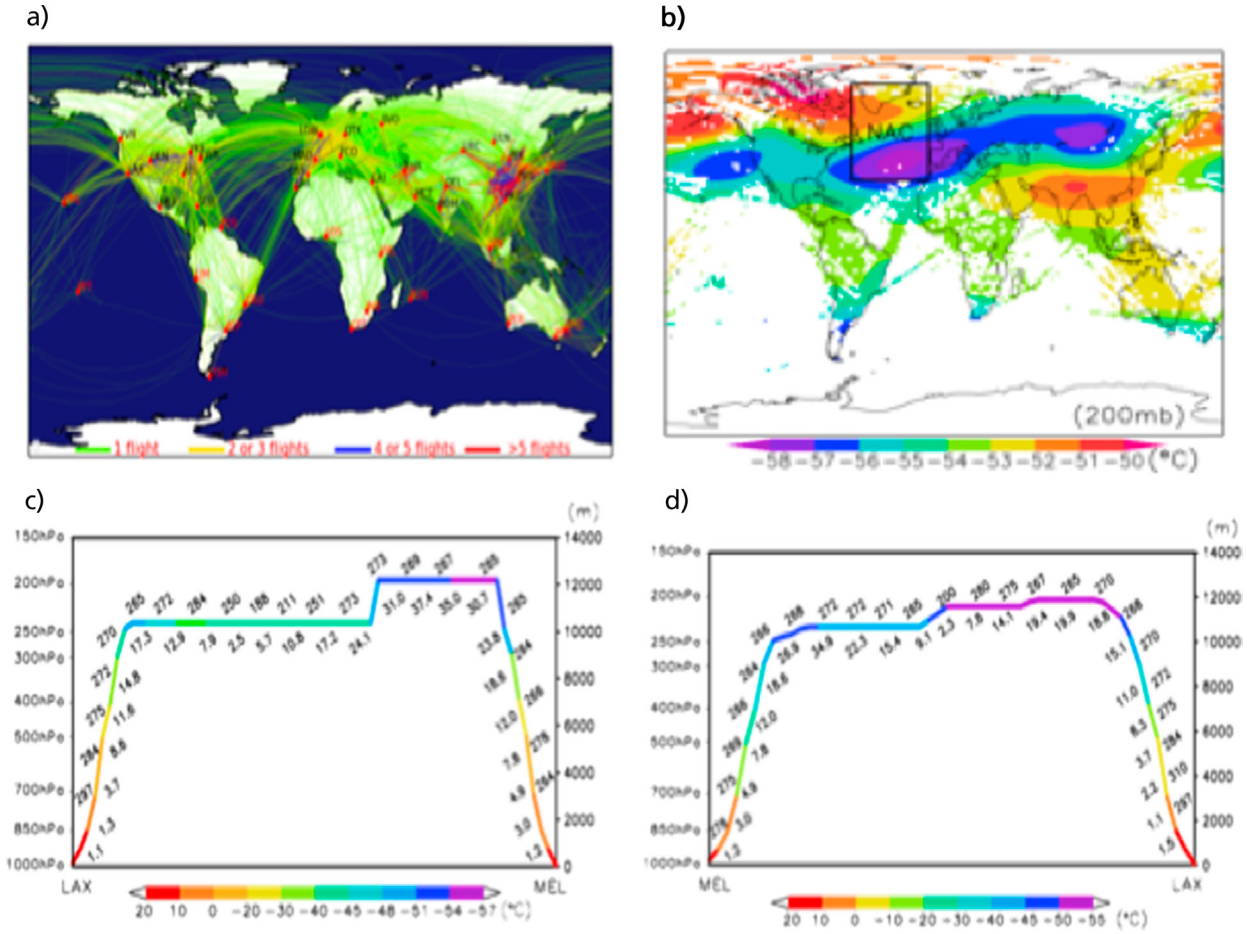

Fig. 1. (a) Publicly available commercial flights for a typical day (16 Jun 2010). Direct flights with multiple sorties are labeled with colored lines. Great circle connections are used instead of actual flight trajectories. The top 50 airports are labeled with their Air Traffic Interface Access (ATIA) IDs. The commercial ticketing inventory also provides carrier aircraft type. The corresponding mechanical parameters are used in the estimation of drag changes using along-the-route integration method. (b) The 200 hPa air temperature (ERA-Interim) experienced by the commercial flights, using a mask from (a) but of 1.25° × 0.94° footprint size. Especially in the Northern Hemisphere, it covers over 70% of the entire airspace. The black box defines the busy aviation corridor NAC. Reichler's (Reichler et al. 2003) scheme is used in determining the intersect of tropopause and 200 hPa surface [thick black line in (b)]. (c) A sample flight trajectory from Melbourne to Los Angeles on 1 Jan 2010. Primary vertical axis is pressure. The secondary vertical axis is altitude. Horizontal axis is time normalized by the total flight time (0–1) for the complete seven stages. Colors on the line segment indicate the temperatures experienced. To avoid the jet stream, the aircraft chose a lower cruising level altitude for a significant period of time. (d) For comparison, the reverse flight, from Los Angeles to Melbourne. To benefit from the jet stream tailwinds, a typical 200 hPa cruising level was chosen. Wind speed and directions are labeled along the track. In (c) and (d) the U.S. standard atmosphere is used to convert altitudes into pressure levels. The standard meteorological approach to measuring wind direction (starting from due north and positive counterclockwise) is used.

increased speed is the more dominant term. Other likely manifestations of climate change, such as more strongly sheared upper-level jets, are expected to affect turbulence and therefore passenger comfort and safety (e.g., Williams 2017; Williams and Joshi 2013; Sharman et al. 2006; Storer et al. 2017). However, the net effects of changing wind patterns on fuel consumption, at least for round-trip flights, currently appear to be minor. In this study, the fuel efficiency issue is elucidated from the perspective of what flying through a warmer atmosphere would be like, in the near future.

It has been found that an elevated tropopause height (e.g., Santer et al. 2003; Reichler et al. 2003; Lorenz and DeWeaver 2007) incurs additional fuel cost due to the extra potential energy

Downloaded from http://journals.ametsoc.org/bams/article-pdf/101/10/E1761/5013924/bamsd190239.pdf by guest on 24 November 2020

required in climbing to higher altitudes. However, this cost is relatively small, especially for long-haul flights, because the cruising stage is the most fuel consuming (Ren and Leslie 2019a). For the high radiative forcing representative concentration pathway 8.5 W m^{-2} (RCP8.5) scenario (Taylor et al. 2012), thermal efficiency reduction, as a consequence of increased environmental air temperature, can reach ~0.3% for a large global area over a 100-yr period (e.g., between two 20-yr periods centered respectively 1980 and 2080; Ren and Leslie 2019b). However, there is a significant counter effect from increased mechanical (thrust) efficiency, so the net reduction in fuel efficiency is only ~0.02% (Ren and Leslie 2019a) for current engine technology and may be even less in the future higher turbine entry temperatures (TETs).

Ren and Leslie (2019a), using a line-by-line integration from a commercial passenger flight inventory, found that the net effect of warming is a reduction of fuel efficiency. Here, the underlying physics is further explained and future trends of climate warming impacts on fuel efficiency are assessed. By analyzing atmospheric parameters from multiple climate models, this contribution focuses on obtaining a reliable range for changes in skin friction drag, which is a far larger component of fuel costs than thermal efficiency and elevated tropopause levels. The article is organized as follows. The governing equation for body drag is presented in the "Bernoulli aviation invariant" framework. Air viscosity, because of its unique character, is selected as a physically sound index for fully representing fuel efficiency changes in a warming climate. The well-known, canonical Sutherland equation (Chapman and Cowling 1970) is applied to the three-dimensional temperatures from 34 state-of-the-science climate models (Table 1). Statistically reliable conclusions are possible because projected air temperature, as a primary atmospheric parameter, has the highest intermodel consensus of all key variables [see, e.g., IPCC Third Assessment Report (TAR) and subsequent IPCC assessment reports; Sausen et al. 2005]. The ensemble character of changes in air dynamic viscosity in the cruising space are analyzed and the uncertainty is quantified. Percentage changes in frictional drag are shown for six simulated flights over diverse climate zones. Finally, using publicly available commercial flight records and the standard seven-phase flight profile (Fig. 1), the global effects

Table 1. The 34 climate models (GCMs) used in this study. The asterisk (*) and the dagger (†) indicate two ensemble sets of a 27-member and a 16-member climate models.

Name	Institution	Grid stencils (lon/lat/vertical)	Name	Institution	Grid stencils (lon/lat/vertical)
*ACCESS1-0†	BoM, Australia	192 × 144 × 17	GFDL-ESM2G	GFDL, United States	144 × 90 × 17
*ACCESS1-3†	BoM, Australia	192 × 144 × 17	*GFDL-ESM2M†	GFDL, United States	144 × 90 × 17
BCC_CSM1.1†	CMA, China	128 × 64 × 17	*GISS-E2-R	NASA, United States	144 × 90 × 17
*BCC_CSM1.1(m)	CMA, China	320 × 160 × 17	*HadGEM2-CC†	MOHC, United Kingdom	192 × 144 × 23
BNU-ESM	BNU, China	128 × 64 × 17	HadGEM2-ES†	MOHC, United Kingdom	192 × 144 × 17
*CCSM4†	NCAR, United States	288 × 192 × 17	IPSL-CM5A-LR	IPSL, France	96 × 96 × 17
*CESM1-CAM5	NDN, United States	288 × 192 × 17	*IPSL-CM5A-MR	IPSL, France	144 × 143 × 17
CMCC-CM	CMCC, Italy	480 × 240 × 17	*MIROC-ESM-CHEM	NIES, Japan	128 × 64 × 35
CMCC-CMS	CMCC, Italy	192 × 96 × 33	*MIROC-ESM	NIES, Japan	128 × 64 × 35
*CNRM-CM5†	CNRM, France	256 × 128 × 17	*MIROC5†	AORI, Japan	256 × 128 × 17
*CSIRO-Mk3.6.0	CSIRO, Australia	192 × 96 × 18	*MPI-ESM-LR†	MPI, Germany	192 × 96 × 25
*CanESM2†	CCCma, Canada	128 × 64 × 22	*MPI-ESM-MR	MPI, Germany	192 × 96 × 25
*FGOALS-g2†	IAP, China	128 × 60 × 17	*MRI-CGCM3†	MRI, Japan	320 × 160 × 23
*FGOALS-s2†	IAP, China	128 × 108 × 17	*INM-CM4	INM, Russia	180 × 120 × 17
*FIO-ESM	FIO, China	128 × 64 × 17	*NorESM1-M	NCC, Norway	144 × 96 × 17
*GFDL-CM3†	GFDL, United States	144 × 90 × 23	*NorESM1-ME	NCC, Norway	144 × 96 × 17
*CESM1-BGC	NSF–DoE–NCAR (NDN), United States	288 × 192 × 17	*HadGEM2-AO†	KMA, South Korea	192 × 144 × 17

Downloaded from http://journals.ametsoc.org/bams/article-pdf/101/10/E1761/5013924/bamsd190239.pdf by guest on 24 November 2020

of fuel costs are estimated out to year 2100. The analyses presented here are intended to be robust as they all are unified under just one primary, simple to interpret, fuel cost expression.

Methods, data sources, and processing

The following analyses are based on the assumption that the current, primarily mechanically, aviation technology is not expected to experience major transformative changes during the twenty-first century. This hypothesis is supported by the future plans of major engine builders and aircraft manufacturers. Over the past century, after technology advanced from piston engines to turbofans, the limit of thermal breathing engines is being approached. Perfecting electrification and achieving environmental goals are the major current themes of the aviation industry. Federal Aviation Administration (FAA) regulations also are assumed not to experience future major adjustments so that the majority of commercial aircraft still cruise at altitudes around 100–300 hPa (e.g., Lee et al. 2019); and it is expected that the same seven-stage flight profile will hold. In this study, the conclusions are universally applicable to all types of aircraft that cruise at these high altitudes. These fundamental, physics-based conclusions are intended to assist in the preparation of adaptation measures in a warming climate.

Governing equations for frictional drag and viscosity. For both laminar and turbulent flows, frictional drag ($F\tau$ the lateral force exerted by stress τ) exerted by the environmental air on aircraft is proportional to the dynamic air viscosity (μ):

$$F\tau = AC_D\rho_a\left|\mathbf{V}_0\right|^2 = AC_D^*\mu\dot{\varepsilon}\left(\rho_a, \mathbf{V}_0\right), \tag{1}$$

where A is effective total surface area, ρ_a is reference air density (undisturbed environmental air density), $\mathbf{V}_0$ is the velocity of the aircraft, and the dimensionless drag coefficient C_D includes the interaction of the approaching air particles with the surface they impinge upon. Thus, the frictional drag is partly a technology-determined constant, C_D^*, the properties of the aircraft surface, and proportional to air dynamic viscosity, μ, embodying property of the approaching air particles. For a fixed design, the same cruising speed produces different shear strain rates $(\dot{\varepsilon})$ of the ambient air, for different air densities. However, the shear rate is linearly proportional to the aviation invariant (Ren et al. 2018), like other performance parameters such as lift and pressure drag. From Eq. (1), for a given transportation capacity the effects of environmental warming on body drag are completely representable by changes in dynamic viscosity. The effect of air density enters only through the Bernoulli invariant ($\rho_a|\mathbf{V}|^2$). This greatly simplifies the analyses because 1) among current climate model simulated future atmospheric parameters, air temperature, referred to as "T_a" in the IPCC archives, has the highest intermodel consensus; 2) μ is an increasing universal analytical function of T_a, as detailed below; and 3) as a primary parameter, all climate modeling centers output values of T_a, thereby providing a sufficiently large ensemble size for statistically significant conclusions.

It is instructive to consider the thermal agitation (of carriers of electricity) in increasing electric resistance and the temperature increase in increasing gas viscosity, because both are rooted in the same fluctuation–dissipation theorem. According to the Sutherland equation (Chapman and Cowling 1970), air viscosity is

$$\mu = bT_a^{1.5}/\left(T_a + S\right), \tag{2}$$

where T_a is air temperature (K), $b = 1.458 \times 10^5$ kg m^{-1} s^{-1} K$^{-0.5}$, and $S = 110.4$ K. Using the U.S. standard atmosphere, a simple sensitivity experiment is performed to assess the impact of a 1.5°C warming, uniformly distributed along the vertical stratification profile. It is found that there is a 0.5%–0.8% increase in dynamic viscosity (Fig. 2). Dynamic viscosity can

Downloaded from http://journals.ametsoc.org/bams/article-pdf/101/10/E1761/5013924/bamsd190239.pdf by guest on 24 November 2020

vary over a 30% range in the lower 80 km of Earth's atmosphere. Flying within the thin isothermal layer at ~10–15 km above mean sea level (MSL), which is close to the tropopause altitudes, enjoys not only the highest thermal efficiency, but also the least viscous atmosphere. From Eq. (2), dynamic viscosity is an increasing universal function only of air temperature, permitting a succinct analysis of climate warming effects on fuel efficiency, and hence environmental footprint size. There is a close interaction between aviation and global climate change in the twenty-first century. This is partly because the radiative effects from tracers in the exhaust, such as water vapor, CO_2, NO_x, and various oxides of the halogen family elements, will have direct thermal consequences for temperature stratification in the upper troposphere and lower stratosphere (UTLS). However, as tracers, their direct effects on viscosity are negligible, as the perturbations of viscosity values would be ~11 orders of magnitude smaller than the base values calculated from a base state atmosphere dominated by N_2 and O_2. Also, the densest air traffic is in the midlatitudes (Fig. 1b), especially in the Northern Hemisphere. Midlatitude, natural cirrus clouds can be influenced by the aircraft induced contrails (IPCC 1999, 2013), and there is an increasing trend (Lee et al. 2009). This is considered to be responsible for much of the aviation impact on climate (Voigt et al. 2017) and would have direct effects on the temperature at the cruising altitudes. Unfortunately, the radiative impact of cirrus has not been well quantified thus far; in particular, the solar albedo effect of the ice particles still is not clear (e.g., Chen et al. 2000). Despite active investigations such as the Midlatitude Cirrus experiment (ML-CIRRUS), the current state of the science measurement of UTLS vapor and tracers, there remains considerable uncertainty in accurately delineating between natural cirrus and the contrail cirrus. Considering the difficulty in predicting the atmospheric heating from contrails (e.g., Liou 1986), the present study will consider only the temperature trends available from the Fifth Assessment Report (AR5) scenario runs.

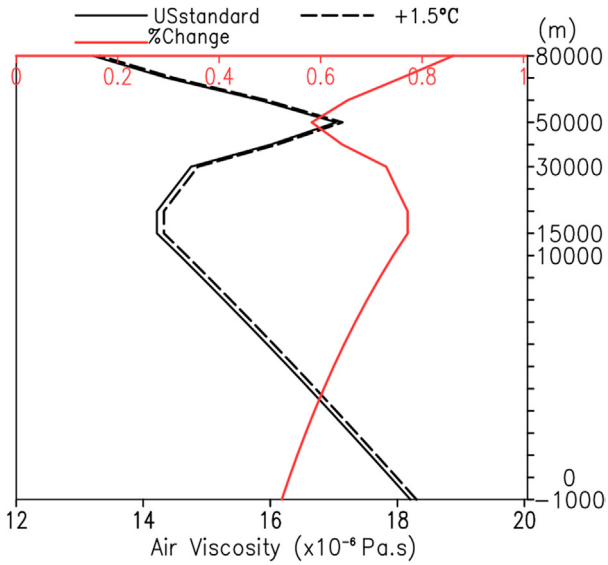

Fig. 2. Effects of a 1.5°C temperature increase on atmospheric viscosity (red line, percentage increments). Viscosity values are estimated from the Sutherland equation [Eq. (2)]. Black thick line is from the U.S. standard atmosphere stratification. Dashed lines are from the 1.5°C uniform perturbation of the vertical temperature profile. Red line shows the changes in percentage. For the U.S. standard atmosphere, the increase in dynamic viscosity can range from ~0.5% at the ground to ~0.85% at 80 km MSL. The 1.5°C Paris Climate Change Agreement upper limit is used here for illustrative purposes.

Climate model output. In this study, dynamic air viscosity and its variations in the cruising altitudes are examined over the twentieth and twenty-first centuries, estimated using 3D air temperatures from 34 climate models. Based on these analyses, the increased body drag is examined and the intermodel spread of the uncertainty assessed up to 2100. The largest uncertainty in the extent of warming resides with the industrial emission of greenhouse gases (GHGs) and other pollutants in the atmosphere, to which climate is sensitive to the additional radiative forcing (Lewis and Karoly 2015). The future state of the climate will depend crucially on what emissions controls the various nations decide to impose (Dessler 2010). In the most recent IPCC assessment report (AR5), the driving scenario is in the form of RCPs. Here the climate model outputs under the high emissions scenario RCP8.5 are used. The climate model outputs of air temperature are obtained from the IPCC Deutsches Klimareshenzentrum (DKRZ) Data Distribution Centre (www.ipcc-data.org/sim/gcm_monthly/AR5/Reference-Archive.html). For models providing multiple perturbation runs, only r1i1p1 runs are used, meaning all

Downloaded from http://journals.ametsoc.org/bams/article-pdf/101/10/E1761/5013924/bamsd190239.pdf by guest on 24 November 2020

ensemble members use the same initial conditions and the same physical parameterizations (Taylor et al. 2012). Details of each climate model and the availability of output parameters are available online (http://cmip-pcmdi.llnl.gov/cmip5/availability.html).

There are 34 climate models that have archives of their respective historical (e.g., 1850–2006) and scenario (e.g., 2006–2100) runs (Table 1) in phase 5 of the Coupled Model Intercomparison Project (CMIP5). For clarity, a subset of these models can be presented as representatives in the following discussion. They are chosen primarily because they are from independent modeling centers, and also because the authors have accumulated considerable experience with the systematic bias of the models from several previous studies (e.g., Ren and Leslie 2015; Ren 2010). During the twentieth century historical runs, the time series of model generated geopotential heights, specific humidity, and air temperatures all have systematic biases but the trends satisfactorily represent reality, compared with NCEP–NCAR reanalysis data (e.g., www.esrl.noaa.gov/psd/data/gridded/data.ncep. reanalysis.html), for both polar (Ren et al. 2011) and lower-latitude regions (Ren and Leslie 2015).

Commercial flight legs. Aviation is exposed to atmosphere levels up to the UTLS (Figs. 1b–d). Analysis of the stresses experienced during the entire flight profiles is necessary. According to FAA regulations, the flight profile comprises seven stages (viz., A–G; ranging from taxi-out to taxi-in). To estimate the additional work needed, an along-flight route integration is the best approach [see Eq. (3) of Ren and Leslie (2019a) and "A unified expression for in-flight fuel burning" section for a unified inflight fuel cost formulation]. Because the commercial data on all flight logs are not publicly available (e.g., over China and India), some assumptions are necessary, according to the carrier aircraft and the routes. The publicly accessible flight logs are available online (e.g., OpenSky Network at https://opensky-network.org/data/impala). The Impala shell was used to selectively obtain the publicly available flight control data from OpenSky Network. For example, the flight tracks in Fig. 1a and the sample flight logs in Fig. 1c are used to determine the cruise altitudes of flights of various ranges. Compared with peer flight trackers, OpenSky Network is known to have higher data quality due to its quality control (QC) procedures (https://openflights.org/data.html#route). The OpenSky records and commercial ticketing inventories are cross-checked to determine the actual carrier aircraft. The mechanical parameters and geometry of carrier aircraft are publicly available.

A unified expression for in-flight fuel burning. Detailed scientific results and crucial lessons learned from past research are described below. Fuel burning efficiency is a relatively new concept. Hence, a brief introduction to the aircraft force balance during all stages of flight, and the respective factors affecting fuel burning seems necessary for readers to understand the basics of aviation fuel burning, and to assist in interpreting the ideas presented in the subsequent discussion.

The drag (D) and thrust (T) and the lift (L) and weight (W) are two pairs of force acting on an aircraft during all stages of the flight. Typically, the magnitudes of D and T are much smaller than L and W. That is, the L-to-D ratio of aircraft at cruising altitude usually is in the range 10–20. The generic form of drag, $D = PA\sin\alpha + \tau A_0 + R$, and lift, $L \approx PA\cos\alpha$, involve the attack angle α (rad), skin friction τ (Pa), flying-direction normal pressure relief R (Pa), net normal pressure difference across wing (and fuselage) P (Pa), wing span area A (m^2), and total surface area A_0 (m^2). Thrust (T) is an important engine aerodynamic property (adjustable during flights, root cause of acceleration and deacceleration). Total weight at a particular moment is $W(t) = g(M_0 + M_e + m_f)$, where g is the gravitational acceleration ($m\ s^{-2}$), M_0 is the empty aircraft weight (kg), M_e is the effective payload (kg), and m_f is the instantaneous total fuel weight (kg). During flight, m_f is the only component of total weight that varies. Consequently,

Downloaded from http://journals.ametsoc.org/bams/article-pdf/101/10/E1761/5013924/bamsd190239.pdf by guest on 24 November 2020

the fuel burning rate also is the total weight loss rate: $\dot{m}_f = -\dot{W}/g$. The level flight at cruising stage, the fuel burning rate can be written as

$$\dot{m}_f = \frac{DV_c}{\gamma\bar{\eta}}, \tag{3}$$

where V_c is the cruising speed (m s^{-1}), γ is the specific energy of jet fuel, and $\bar{\eta}$ is the overall engine efficiency (which can be further decomposed as the product of mechanical and thermal efficiency; Ren and Leslie 2019a). At the cruising stage, assuming α is very small, the expression for D can be simplified significantly. A time integration of Eq. (3) is used in the estimation of fuel cost, with geometrical and mechanical parameters (including the specific energy of fuel) obtained from the Jane's All the World's Aircraft (https://ihsmarkit.com; https://web.archive.org/web/20150907173111/https://www.cgabusinessdesk.com/document/aviation_tech_review.pdf) and other references, including Mattingly et al. (2002) and Tennekes (2009). During the take-off and landing stages, the forces in the horizontal and vertical directions are not in balance and there are accelerations (and generation of kinetic energy and potential energy). The fuel burning rate is significantly greater than the level cruising fuel burning rate in Eq. (3). The fluctuation range is limited by FAA regulations. It therefore is necessary to separate out the potential and kinetic energy terms in the temporal integration. The (minimum) total work an aircraft needs to perform from the originating to the destination airport is

$$W_{\text{Total}} = \text{KE} + \Phi + \gamma \int_{\substack{\text{flight}\\ \text{period}}}^{\text{entire}} \dot{m}_f \, dt, \tag{4}$$

where KE and Φ are respectively the kinetic energy and potential energy of the aircraft after climbing has ceased, and $\dot{m}_f$ is level cruising burning rate. The descending stage potential energy is assumed not to be reclaimable. The total fuel mass cost during a flight then is $\Delta m_f = W_{\text{Total}}/\gamma$.

Also from Eq. (3), the cruising stage fuel burning is used to overcome horizontal drag. This explains why headwinds do not necessarily result in greater fuel costs than tailwinds, as might be expected from an increase in flight time. For example, a reduced attack angle can increase thrust efficiency and hence overall engine efficiency. Careful derivation indicates that on time arrival of a flight experiencing headwinds increases fuel costs. However, increasing the flight times can reduce the profit loss (and may even benefit from headwinds). The drag at this stage still is composed with normal and lateral components. Some normal component is related with lift and some are resistance (e.g., R, which is much less than P but typically is larger than, or of the same magnitude as, τ). In airplane geometry design, R and τ alternate as reducing one usually requires increasing the other (a type of Betz's law in aerodynamics). But only τ is sensitive to climate change [Eqs. (1) and (2)]. Other parameters are either geometry parameters or associated with lift generation and are insensitive to a warming environment. Equation (3) indicates that cruising at the tropopause level not only improves thermal efficiency, but also experiences the lowest air dynamic viscosity, which is directly proportional to its body drag. From Eq. (3), any factors affecting overall efficiency $\bar{\eta}$, skin friction τ, and possible flying length can affect fuel consumption. Flight time and distance can vary for a number of reasons, including to avoid severe weather (e.g., Williams 2016). In the following discussion, the subsection division is based on this reasoning.

In a simple to understand manner, Eq. (3) also indicates that neither microscopic nor macroscopic mechanisms alone can fully address the fuel efficiency issue in a warming future climate; both are needed for assessing this environmental problem. To estimate the fuel efficiency changes by the end of the twenty-first century, using atmospheric temperatures from multiple climate models, Eq. (2) is driven by the air temperatures in the control period

Downloaded from http://journals.ametsoc.org/bams/article-pdf/101/10/E1761/5013924/bamsd190239.pdf by guest on 24 November 2020

(1950–2000) and the prediction period (2050–2100), to obtain dynamic viscosity values for both periods. Global patterns of viscosity changes then are analyzed. To estimate extra fuel costs if the present civil aviation activity persists through the twenty-first century, integrations along idealized seven-stage flight profiles are performed for all flights recorded in the year 2010 commercial flights inventory. Multiple legs flights are separated into adjacent direct flights, each with their respective seven-stage profile. Ensemble averages are taken after the along-trajectory integrations, driven respectively by all climate models. Using six simulated flights, representing various climate zones, the percentage changes in fuel efficiency also are calculated.

Results and discussion

Using atmospheric parameters provided by the CMIP5 climate models, and the flight and carrier aircraft information provided by a commercial air-ticketing database, global patterns of fuel efficiency changes are investigated. From Eq. (4), the impacts on fuel efficiency are assessed from five aviation consequences of climate change. These are the elevated tropopause height ("Fuel cost impacts of an elevated tropopause height" section), thermal efficiency ("Fuel efficiency from thermal efficiency" section), mechanical efficiency ("Fuel efficiency from mechanical efficiency" section), and body drag ("Fuel efficiency from body drag" section). Finally, other climate warming manifestations that likely have consequences for fuel efficiency are discussed briefly in the "Possible fuel efficiency impacts of other manifestations of climate warming" section. Multiple model ensemble (MME) mean temperatures from 27 of the 34 climate models are used in the analyses (Table 1, marked with asterisks). All climate models are interpolated to a 1.25° × 192 latitudinal Gaussian grids horizontal resolution before calculating the ensemble mean, to facilitate cross-model comparison and intermodel spread estimates.

Fuel cost impacts of an elevated tropopause height. Figure 3 shows the absolute changes (in m) in the 200 hPa geopotential heights between the control and the projection periods, under the RCP8.5 emissions scenario. From this figure, it is apparent that the 200 hPa geopotential height was elevated by 150 m (ranging from 50 to 260 m) over the 100-yr period, globally. The incurred extra fuel cost is only ~0.04% of the total fuel consumed for a >1,000 km flight. A comparison of Figs. 3 and 4 reveals that the results for the RCP4.5 scenario differ only quantitatively from RCP8.5.

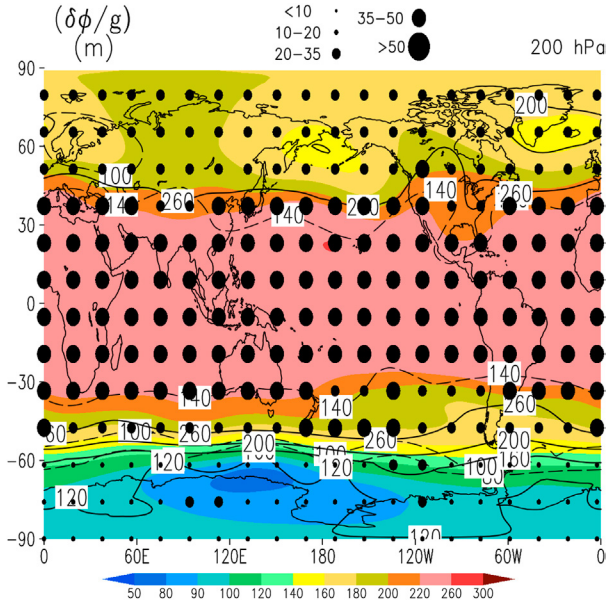

Fig. 3. Geopotential height changes (color shades in meters) between the historical period (1950–99) and the projection period (2050–99, under the RCP8.5 scenario), estimated from 27 climate model ensemble geopotential heights at 200 hPa. Solid lines and dashed lines are upper and lower envelopes of the ensemble estimates of geopotential height changes. Black dots are intermodel spread, defined as the across-model standard deviation (rms). Five bin levels of rms are used (shown as dots of different sizes).

Fuel efficiency from thermal efficiency. The thermal efficiency of aircraft engines is adversely affected by environmental temperature increase. The second law of thermodynamics places a fundamental limit on the thermal efficiency (η_T), as presented in Eq. (1) of Ren and Leslie (2019a):

$$\eta_T = \varepsilon\left(\mathrm{TET} - T_C\right)/\mathrm{TET}, \tag{5}$$

where ε is a technical limiting factor indicating the proximity of the actual engines to the ideal

Downloaded from http://journals.ametsoc.org/bams/article-pdf/101/10/E1761/5013924/bamsd190239.pdf by guest on 24 November 2020

engine (Holman 1980), and T_C is the absolute temperature of the exhaust gases; T_C closely follows the environmental air temperature T_a, with only a cooling technology-dependent constant difference. Figure 5 shows the global distribution of engine thermal efficiency decrease $\left(\eta_T/\eta_T^o\right)-1$ between the control $\left(\eta_T^o\right)$ and the projection periods (η_T), for the RCP8.5 forcing scenario, assuming a TET of ~1,800 K. Global distribution patterns generally are zonal, with a more significant decrease at lower latitudes, reaching 0.6%. Thermal efficiency decreases in the busy 20°–60°N belt, at ~0.2%–0.6%. The polar regions experience increased thermal efficiency, which is of minor importance as most airlines do not traverse these regions. Figure 6 applies to RCP4.5, which has smaller magnitudes but the general geographic patterns are very similar to those of RCP8.5. The intermodel spread generally is less than 20% of the mean values of efficiency changes. The zonal pattern of thermal efficiency decrease is persistent, with the tropical and lower latitudes showing the most significant loss of thermal efficiency.

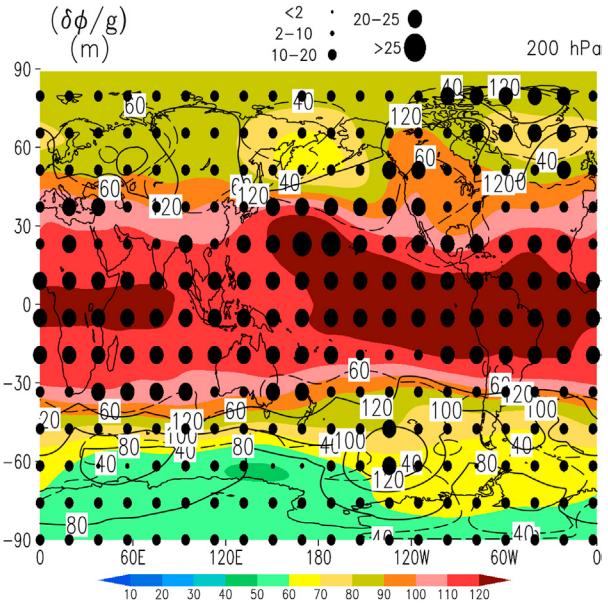

Fig. 4. As in Fig. 3, but under the RCP4.5 emissions scenario.

Fuel efficiency from mechanical efficiency. As the airplane moves forward by ejecting exhaust backward, how the kinetic energy, which is extracted from the fuel-burning chemical energy, is partitioned between the aircraft and the exhaust jet (i.e., used for pushing aircraft forward versus removed by the exhaust) is measured by the mechanical (propulsive) efficiency (η_M):

$$\eta_M = 2/\left(1 + V_e/V_a\right), \tag{6}$$

where V_e is effective exhaust speed (jet speed relative to airplane), and the airplane speed V_a is relative to the ground. Changes in propulsive efficiency over the projection period (η_M) and control period $\left(\eta_M^o\right)$ is defined here as $\left(\eta_M/\eta_M^o\right)-1$. Figure 7 is the global distribution of mechanical efficiency increase, for the RCP8.5 emissions scenarios. Figure 8 shows the quantitatively similar patterns of mechanical efficiency changes under the weaker emissions scenario RCP4.5. Mechanical efficiency is affected oppositely to the thermal efficiency. In the mid–low-latitude regions, the magnitude of mechanical efficiency increase can reach 0.04%–0.3%. Considered jointly with the decreased thermal efficiency, the total engine efficiency decrease therefore is ~0.02%. The pattern of mechanical efficiency increase also is largely zonal, with tropical regions profiting

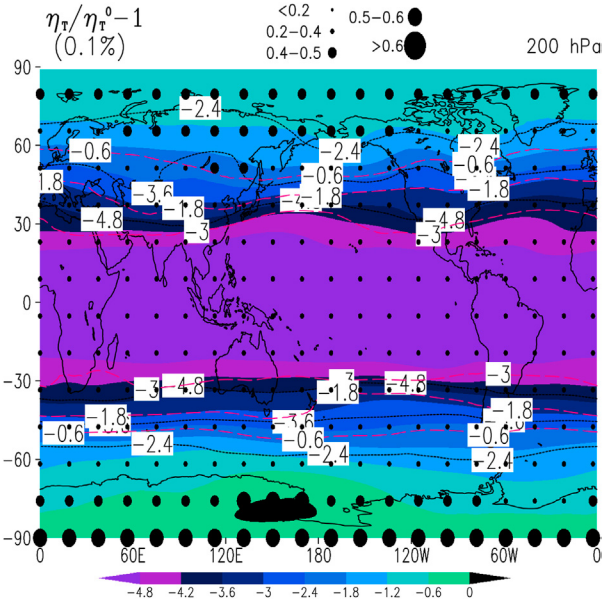

Fig. 5. Cruising altitude (200 hPa) thermal efficiency changes between the historical period (1950–99) and the projection period (2050–99, under the RCP8.5 emissions scenario), from 27 climate model ensemble temperatures. An "imaginary" turbo-fan engine of 1,800 K TET is assumed. Black dots are intermodel spread, defined as the across model (the 27 selected models in Table 1, marked with asterisks) standard deviation. The solid lines and dot–dashed lines are, respectively, the upper and lower limits among the models. Dots are thinned every 10 grids in each dimension, for clarity.

Downloaded from http://journals.ametsoc.org/bams/article-pdf/101/10/E1761/5013924/bamsd190239.pdf by guest on 24 November 2020

most from climate warming. The black dots are the magnitude of intermodel spread. They remain an order of magnitude smaller than the base values of efficiency increase. For both thermal and mechanical efficiencies, the variations in the patterns of the rms error (across-model root-mean-square error) values are primarily due to the pattern-mismatches in the climate models in the climate model simulated 200 hPa temperatures. If a different set of 16 models are selected (e.g., those marked with † in Table 1), the patterns of the dots may change significantly (Figs. ES1–ES4 in the online supplement; https://doi.org/10.1175/BAMS-D-19-0239.2), but they still indicate the same general features. Note that, collectively, the elevated tropopause height and the overall efficiency reduction, are only minor contributors and account a fuel efficiency decrease on the order of ~0.03%. Also, the model spread generally is about one-fifth that of the values of the 100-yr differences. Thus, the trend is apparent, but the intermodel uncertainty remains significant. However, in the not distant future, the trend is very likely to exceed the obscurity cast by natural variability.

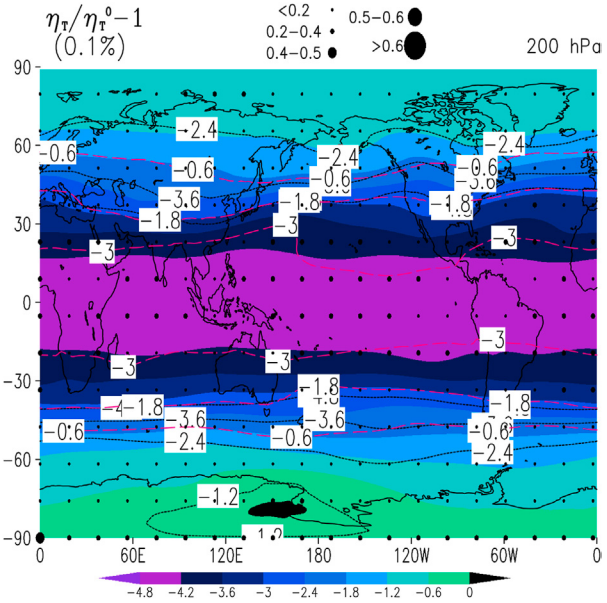

Fig. 6. As in Fig. 5, but for the RCP4.5 emissions scenario.

Fuel efficiency from body drag. The modern climate models indicate a clear consensus on the vertical nonuniformity of climate warming. Climate model predictions of 100-yr warming are calculated using the annual mean for 2050–2100 under the RCP8.5 scenario, minus that for the 1950–2000 historical runs, at 17 standard vertical levels, encompassing the civil aviation flying tracks. Below 250 hPa, warming is a global phenomenon, although it is notable that at very high latitudes, there are cooling areas (e.g., Vallis et al. 2015). However, from Fig. 1a, the very high-latitude cooling areas have little impact on civil aviation. It also is noteworthy that quantitatively there are regional discrepancies among climate models. Around the tropopause zone, approximately 250 to 50 hPa, which includes the typical long-range flight cruising altitudes, there can be significant cooling regions, again mostly poleward of 70° and therefore of little importance for civil aviation. The corresponding air dynamic viscosities and the changes are assessed by applying Eq. (2). For clarity, only 20 models are shown in Fig. 9 and at the 200 hPa level, to represent the cruising altitude of aircraft, justified by the fact that patterns of change are qualitatively persistent between 200 and 50 hPa. Because viscosity is a uniformly increasing function of temperature, the viscosity patterns resemble the temperature patterns. There are

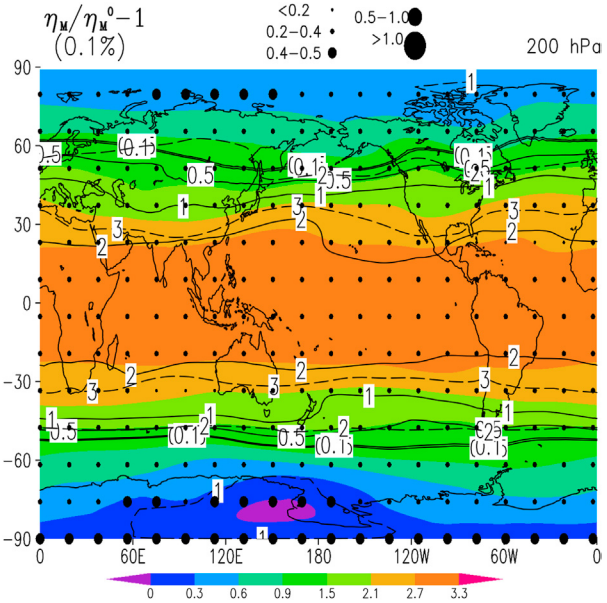

Fig. 7. Mechanical efficiency changes between the historical period (1950–99) and the projection period (2050–99, under the RCP8.5 scenario), from 27 climate model ensemble temperatures at 200 hPa. Black dots are intermodel spread, defined as the standard deviation across the 27 selected models (marked with * in Table 1). The solid lines and dot–dashed lines are, respectively, the uppermost and lowermost values among the models (e.g., at each grid, the highest value among the 27 models. The solid contour lines are generated by this field. Similarly, from the lowest values among the models, the dashed contours are made). Dots are thinned every 10 grids in each dimension, for clarity.

Downloaded from http://journals.ametsoc.org/bams/article-pdf/101/10/E1761/5013924/bamsd190239.pdf by guest on 24 November 2020

very few regions experiencing a viscosity decrease within the band 60°S–60°N. The percentage changes are within 0.5%–1.5% over the 100-yr span. These also are the ranges of frictional drag's percentage changes. Because frictional drag is only a fraction of the total work done by an aircraft [see Eq. (3)], the corresponding change in fuel consumption is ~0.3%. The spatial patterns of viscosity, and the percentage changes over the period, are very similar, which is confirmed by singular value decomposition (SVD; Wallace et al. 1992) analyses of the monthly raw data of viscosity. For example, the models MIROC5 and IPSL-CM5A-LR have very different horizontal resolutions (1.2° vs ~3.75° horizontal resolution) but show very similar spatial patterns of warming at all 17 vertical levels.

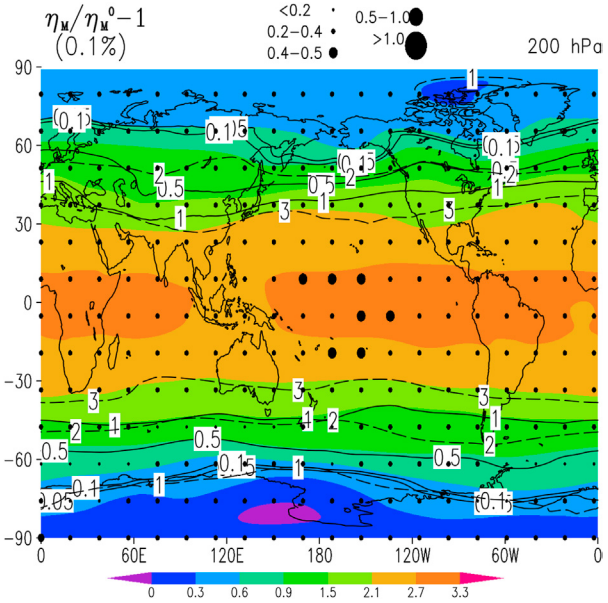

Fig. 8. As in Fig. 7, but for RCP4.5 scenario air temperatures at 200 hPa.

Using an MME is justified also because it is found that, for an arbitrary 20-yr running mean centered on any year between 1900 and 2100, the horizontal spatial temperature patterns are similar between the 34 models, at all model levels encompassing the commercial aviation space. Cross-model similarity also is examined using SVD. The first singular vector from SVD indicated that the temporal correlation coefficient between the monthly temperatures reaches 0.7. Thus, in this case, the MME mean is a better index than individual members. Before performing the inter–climate model statistics, a bilinear interpolation is applied so all climate models are projected to the CCSM4 horizontal grid resolution (~1.25° × 0.94°, latitudinally Gaussian). The changes in viscosity at 150 hPa, included for its proximity to aircraft cruising levels, are shown in Fig. 10. A high degree of intermodel consistency is clearly identifiable: the lower limits (dot lines) closely follow the upper limits (solid lines). At this level, while increased viscosity still is a global phenomenon, the mid to high-latitude regions experience the largest percentage changes.

For the North Atlantic corridor (NAC), defined by Irvine et al. (2013) as located between 30°–75°N and 300°–350°E, the variance of viscosity at aircraft cruise altitudes are shown in Fig. 11, for just 16 selected models, for display clarity. The absolute values of viscosity exhibit wide ranges of intermodel spread. However, the trend from each model exceeds their respective interannual variability. This apparently is due to the drifts in their simulation of air temperature, as was stated earlier. A metric that is not sensitive to temperature climate drifts in model simulations is the normalized time series of viscosity, or the time series normalized by their respective 1900 annual mean values (Fig. 12). The approach adopted in this study determines that the changes in atmospheric fields, rather than climatological means, are important for estimating the changes in fuel efficiency. In that sense, the intermodel spread of their base states (regional extremes of air temperature can reach 3 K), are less important. Using this climate model-drift insensitive index also is necessitated by the fact that, at present, it remains unrealistic to expect climate models to agree with observational reality on a day-to-day basis. Figure 12 shows the normalized time series of viscosity and the intermodel spreads, including multiple model mean, upper and lower limits and the one standard deviation range of the mean time series, over the NAC. By 2100, the body drag likely increases by ~2.2%, compared with 1900. Considering the large annual number flights over the NAC, this corresponds to an extra fuel cost of ~3.8×10^7 gallons annually by 2100, compared with the 2010 reference value.

The above measures are global or regional generic, so specific flight routes have values within those estimates. For six "imaginary" flight routes, flying along the great circle

Downloaded from http://journals.ametsoc.org/bams/article-pdf/101/10/E1761/5013924/bamsd190239.pdf by guest on 24 November 2020

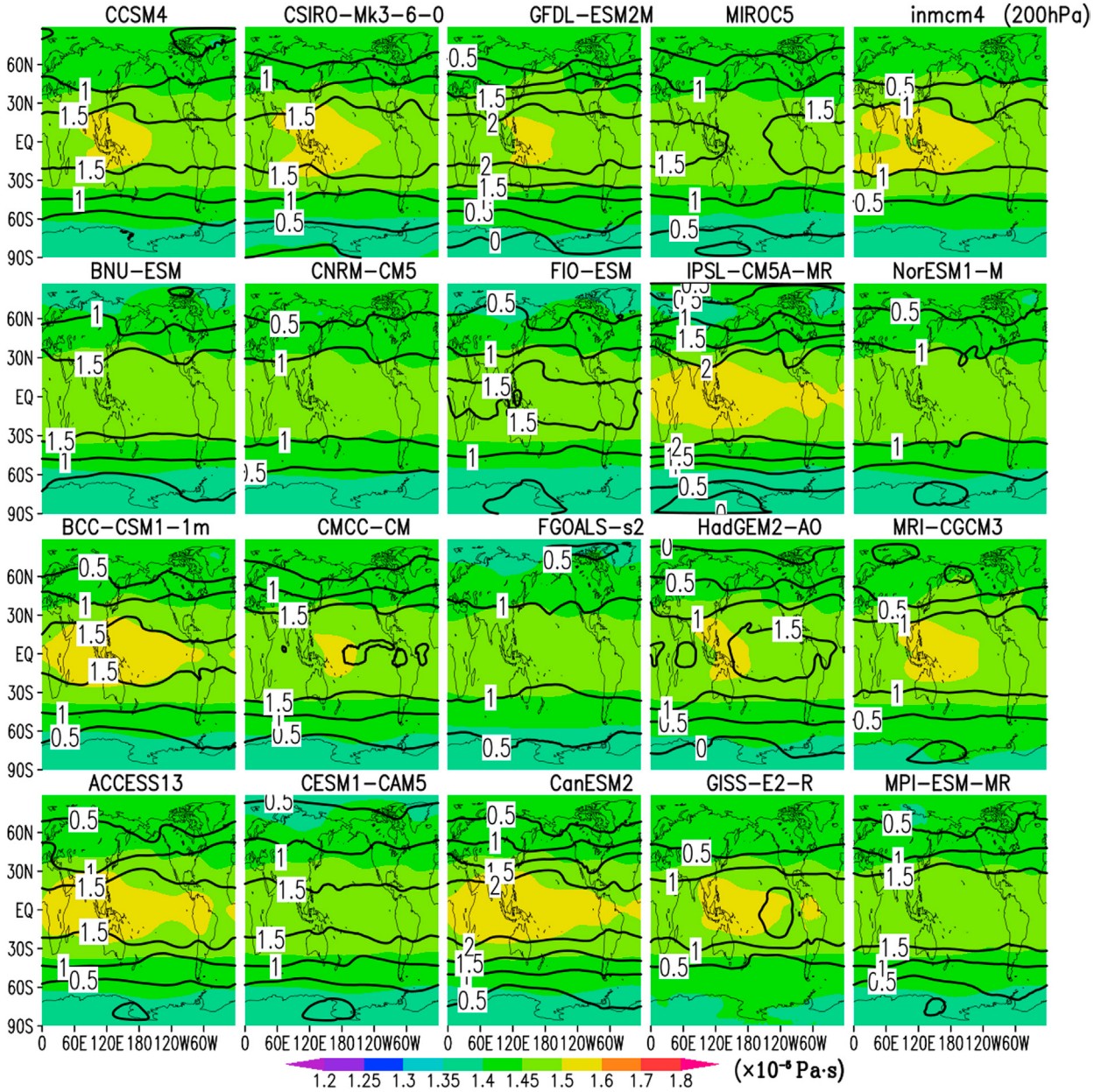

Fig. 9. Air viscosities at 200 hPa derived from 20 climate model simulated air temperatures over the control period (1950–2000, color shades, in 10-5 Pa s). Contour lines are the percentage changes in viscosity between (2050–2100) and (1950–2000). The pattern of changes is vertically persistent (up to 50 hPa) and this level is chosen simply because of its vicinity to the aircraft cruise altitude.

connecting the originating and destination cities, and assuming the seven-stage regulation in the vertical dimension (Fig. 1c), the annual time series of changes in viscosity during the journey are shown in Fig. 13. To emphasize the long-term trend, a 21-point binomial smoother is further applied to the annual time series of the normalized viscosity (figures not shown). The multiple model spread is small compared with the general trend, for each of these routes, typically being within 5% of the mean value. The six flights differ only quantitatively. Generally, flights with most of their cruising tracks in the mid- to low latitudes experience the most significant increase in body drag, reaching ~1.7% century^{-1}.

Here, it is assumed that the current airline routes and the aircraft used to carry out the flights do not change during this period, that is, after 2010. This assumption is necessary because the air temperature warming is nonuniform spatially, both geographically and vertically, in the stratified atmosphere. Analyses carried out here are company by

Downloaded from http://journals.ametsoc.org/bams/article-pdf/101/10/E1761/5013924/bamsd190239.pdf by guest on 24 November 2020

company, aircraft by aircraft, and for all scheduled flights in the year 2010. For each flight, an integration of Eq. (4) along the aircraft trajectory, from takeoff to landing, is made to estimate the drag work, under a current climate and the expected warmer climate in 2100. The differences in work required are converted to equivalent aviation fuel amounts. The along-trajectory integration is rotated for all 34 climate models under the RCP8.5 scenario. The ensemble average is taken among the fuel amounts consumed respectively from being driven by the 34 climate models. The relative changes are shown here as percentages, compared with year 2010. The percentage change in skin friction drag is caused primarily by the increased viscosity of air, within the cruising space, which has a temperature lapse rate of about 8×10^{-8} m^2 s^{-1} K^{-1}. For all operating airlines considered, there is a possible 1.5% increase in skin frictional drag by 2100, whereas the skin friction drag is only a fraction of the total drag [see Eq. (3) of Ren and Leslie 2019a]. The increase in frictional drag accounts for a ~0.22% reduction in total efficiency in fuel consumption, thereby playing a dominant role in the effect of climate on aviation fuel efficiency. Thus, due to increased air viscosity, the annual fuel consumption in 2100 would be ~0.22% higher than around 2010.

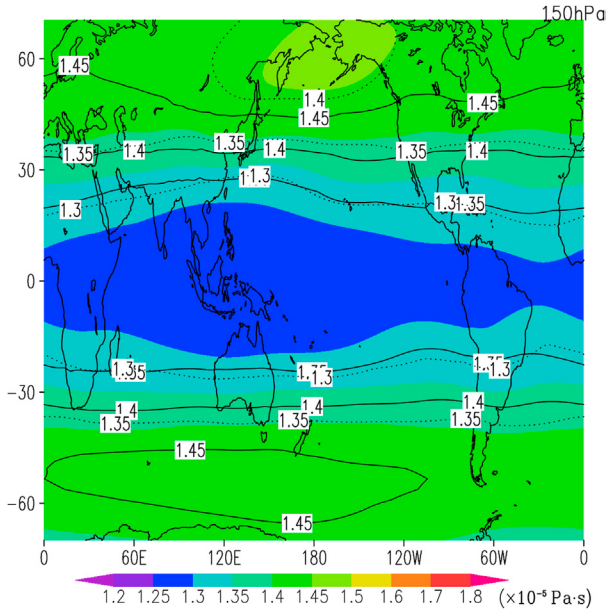

Fig. 10. Multiple (34) climate model ensemble mean air dynamic viscosity (color shades, in 10^{-5} Pa s) at 150 hPa. Upper (solid lines) and lower (dashed lines) limits in the intermodel spread are overlapped to show the high degree of global consistency. All of the model simulated viscosities are bilinearly interpolated to CCSM5 horizontal resolution before the cross-model statistics are performed.

Based on Eq. (5), climate changes induced global jet fuel consumption increases between 2010 and 2100, simulated by 16 climate models from the IPCC AR5 archive, are estimated (Fig. 14). An ~0.22% increase is expected from climate warming alone by 2100, on annual basis. That means a normal year after 2100 would consume an extra ~4×10^6 barrels per year compared with year 2010 (the baseline value of 2010 is 1.825×10^9 barrels per year; www.indexmundi.com/energy/?product=jet-fuel). This is ~1 billion U.S. dollars (in 2010 dollars).

Under the same pressure and temperature conditions, pure tri-atomic gases such as CO_2 and N_2O possess 20% less dynamic viscosity compared with linear molecules O_2 and N_2 (e.g., Turner et al. 1989; Jenkins and DiPaolo 1956). Changes in atmospheric composition certainly will cause changes in viscosity. Sensitivity experiments assuming CO_2 in RCP8.5 and RCP4.5 time series, produced essentially no changes in viscosity. Unlike their radiative properties, which are significant and actually define the vertical temperature profile above the tropopause, the effects on viscosity, derived from Gibbs free energy theory, from each component, follows a log-linear relation of their individual viscosity, with their mole fractions as coefficients. Because the mole fraction of CO_2 and O_3

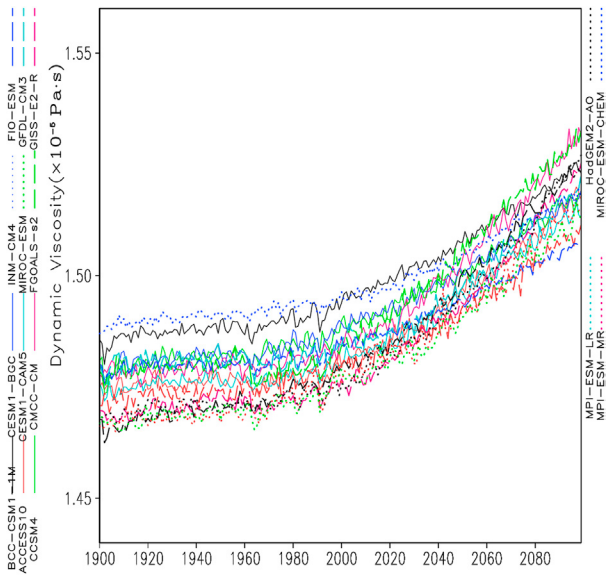

Fig. 11. For the NAC region (30°–75°N, 300°–350°E), the dynamic viscosity simulations are shown for 16 climate models from the IPCC AR5 archive. The annual, intermodel spread still is large. However, for each individual model, the trend far outpaces the interannual and natural variability magnitudes.

Downloaded from http://journals.ametsoc.org/bams/article-pdf/101/10/E1761/5013924/bamsd190239.pdf by guest on 24 November 2020

are so small (<400 ppmv for CO_2 for the lower 50 km Earth atmosphere), their effects on viscosity are many orders of magnitude smaller than a 1°C temperature change. Therefore, compared with the marked effects on viscosity from increased temperature (the optical properties of these tracer gases), the effects from tracer gases on viscosity, are miniscule due to the dominant concentrations of N_2 and O_2. However, their optical and thus thermal effects dominate the stratospheric temperature stratification. The thermal effects presented here are limited to only those represented in the climate models. Aspects not well represented in GCMs include stratospheric warming due to the restoration of the ozone, especially over the Southern Hemisphere [see, e.g., chapters 4 and 5 of the WMO (2018) Scientific Assessment of Ozone Depletion and the references therein].

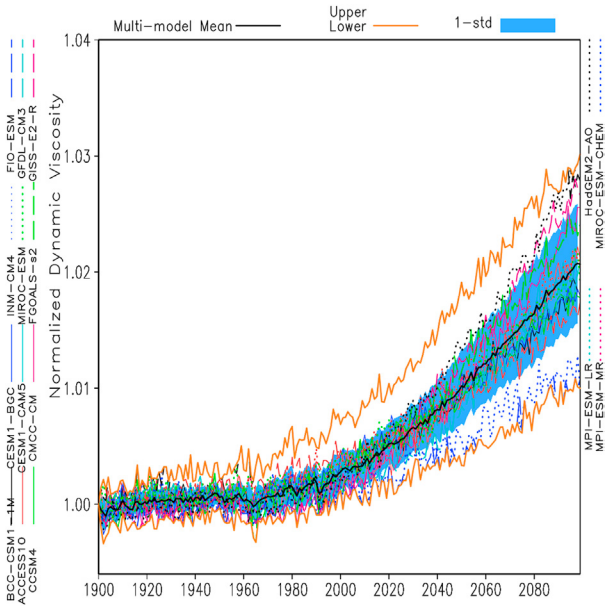

Fig. 12. Normalized dynamic viscosity (averaged over the NAC: 30°–75°N, 300°–350°E) simulated by 16 climate models from the IPCC AR5 archive. Yellow lines define the model spread. Black line is the multiple model mean. The blue envelope denotes one standard deviation around the mean.

Similar analyses were performed for the terms in the "Fuel cost impacts of an elevated tropopause height" to "Fuel efficiency from body drag" sections, based on the European Centre for Medium-Range Weather Forecasts reanalysis, version 5 (ERA5), for the two 10-yr periods 30 years apart (1979–88 and 2009–18). Figures ES5–ES7 are geopotential height and thermal and mechanical efficiency changes from this high-resolution (0.25° × 0.25°) reanalysis. Trends (i.e., 2009–18 mean minus 1979–88 mean) already are evident at present (Figs. ES5–ES7). The regional details are better identifiable than available from the climate models. In particular, the PDO signal is still salient. With increasing time, the zonal distribution of thermal and mechanical efficiencies will become clearer. The change rates of thermal and mechanical efficiencies in ERA5 over the past 40 years already have reached the ensemble climate model mean, for the projection period under the strong RCP8.5 scenario. Features such as tropopause bending, intensified polar jets and associated precipitation changes (e.g., Vallis et al. 2015) are seen in the reanalyses and likely will increase in the future. Other reanalyses were used, including: the NCEP–NCAR reanalysis (e.g., Kalnay et al. 1996); the ERA-Interim (Dee et al. 2011); the NASA Modern-Era Retrospective Analysis for Research and Applications (MERRA; Suarez et al. 2008); and the JRA-55 (Kobayashi et al. 2015), at respectively horizontal resolutions of 2.5°, 0.7°, 0.625° × 0.5°, and 1.25°. They all gave qualitatively similar results.

Possible fuel efficiency impacts of other manifestations of climate warming. From Eq. (3), additional fuel consumption can arise not only from the microphysics-based terms described hitherto, but also from macroprocesses that might increase flying time and distance. These include extended route alterations, resulting from moving to lower or higher altitudes to avoid severe weather, or evading or taking advantage of transitory variations in the location and strength of the jet streams (e.g., Fig. 1c). In extreme cases, aircraft are diverted to other airports. It is difficult to quantify the impacts of these and other likely manifestations of climate change on net fuel consumption. Although not a major component of this study, it is noteworthy that the impacts of climate change on atmospheric turbulence, and hence on passenger comfort and safety, has been increasingly investigated in recent years (e.g., Williams 2017). Atmospheric turbulence also is well known to be one of the major natural hazards for aviation, and has caused severe injuries to both passengers and to the flight and cabin

Downloaded from http://journals.ametsoc.org/bams/article-pdf/101/10/E1761/5013924/bamsd190239.pdf by guest on 24 November 2020

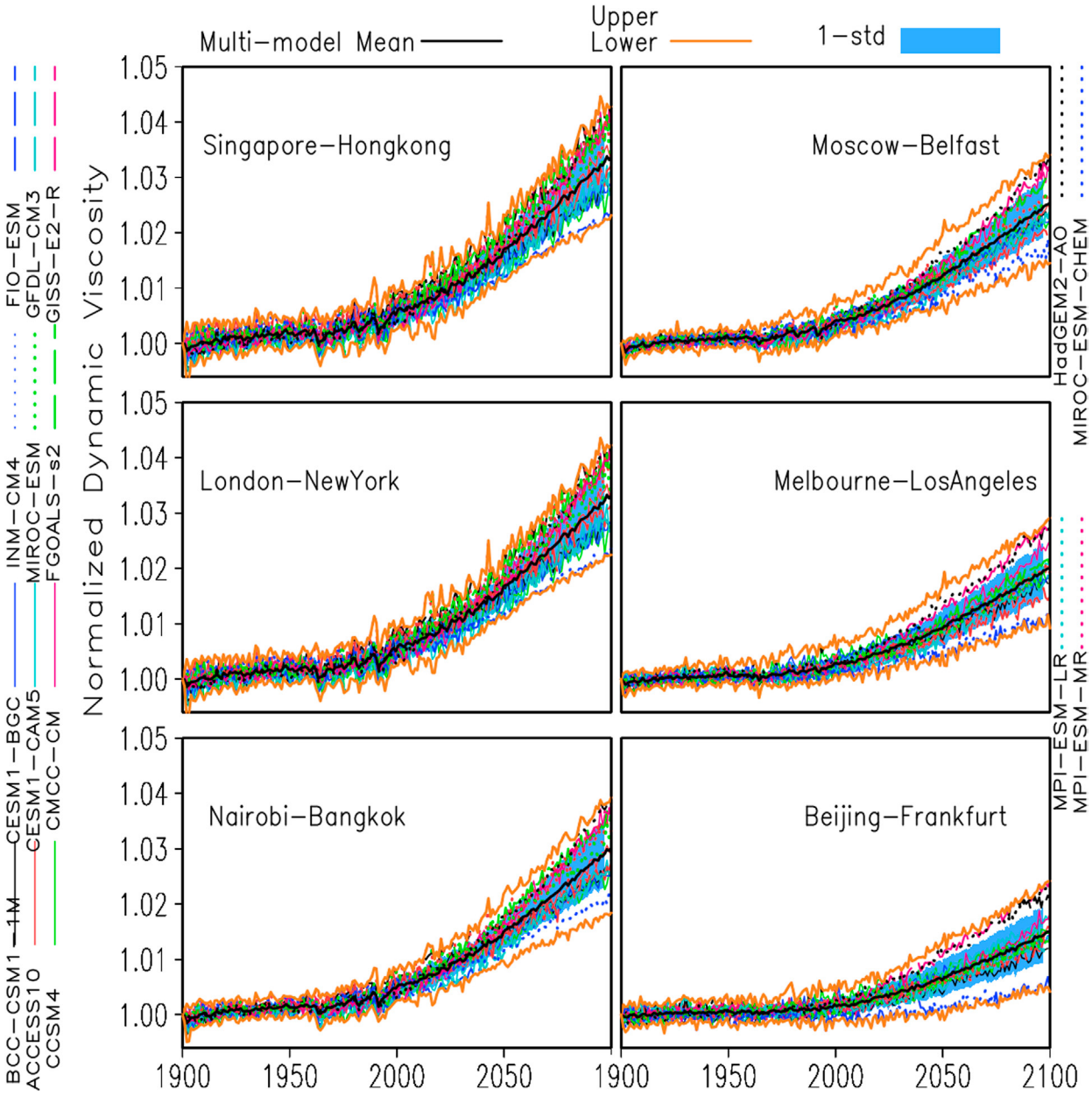

Fig. 13. Body drag increase for six "imaginary" global routes, for illustration. Multiple climate model ensemble means (shown as thick black lines) and the ranges of the variability (thick yellow lines) are shown for 34 climate models under the RCP8.5 emissions scenarios. The blue envelope denotes one standard deviation around the mean.

crew (e.g., Williams 2016, 2017; Storer et al. 2017; Lee et al. 2019). The sources of atmospheric turbulence that affect flights are wide-ranging and highly variable. They include regions of strong vertical shear, severe convection and associated microbursts, and the generation of mountain lee waves (e.g., Doyle 2005) that can propagate both horizontally and vertically. Both severe convection and mountain waves can reach the UTLS, which is the cruising altitude for commercial aircraft (e.g., Sharman et al. 2012a; Storer et al. 2018).

Most studies have focused on the fact that although climate change is decreasing the near-surface temperature difference between the equator and the polar latitudes (Ren 2010), at altitudes near and above the tropopause the temperature difference is increasing. The low altitude decrease is due largely to the greater temperature rises in the near surface polar latitudes than in the lower latitudes. However, contrastingly, at the aircraft cruising altitudes, climate change is increasing the temperature differences between the equator and the poles, resulting from

Downloaded from http://journals.ametsoc.org/bams/article-pdf/101/10/E1761/5013924/bamsd190239.pdf by guest on 24 November 2020

the cooling of the stratosphere in the polar latitudes and amplified warming of the upper troposphere at tropical latitudes (Lee et al. 2019). From the thermal wind equation (e.g., Wallace and Hobbs 1977), the increased thermal gradient will result in greater vertical wind shear near the jet stream, as it is the region of great horizontal temperature gradient. Because high vertical wind shear typically is associated with atmospheric turbulence, various studies suggest that climate warming will increase the occurrence and severity of both clear-air and convective turbulence (Sharman et al. 2012b; Kim et al. 2016; Williams 2016, 2017; Storer et al. 2017; Lee et al. 2019). Despite the demonstrated impact of severe turbulence and jet stream on aviation, as yet the implications for fuel consumption are largely unstudied. However, the impacts can sometimes be of the same, or even larger, magnitude than the viscosity issue that is the focus of the present study. However, flight plan diversions are not as tenacious as global warming (caused viscosity increase) and can be effectively circumvented. One example is permitting higher cruising altitudes. Nevertheless, climate warming impacts on atmospheric turbulence, and hence on passenger comfort and safety, remains a very relevant issue.

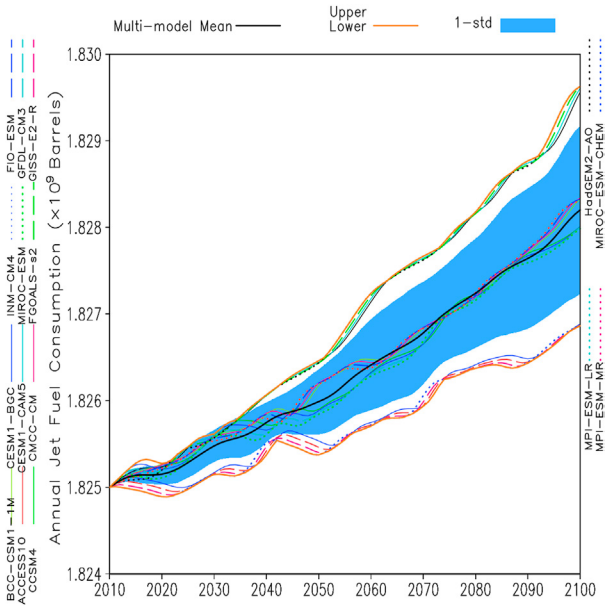

Fig. 14. The global jet fuel consumption increases between 2010 and 2100, simulated by 16 climate models from the IPCC AR5 archive. Yellow lines define the model spread. Black line is the multiple model mean. The blue envelope denotes one standard deviation around the mean. A 21-point binomial smoother was applied to the annual time series. The baseline value of 2010 is 1.825 × 109 barrels per year (www.indexmundi.com/energy/?product=jet-fuel). The FAA regulations and flight routes at 2010 (Fig. 1a) are assumed to remain unchanged.

Notwithstanding the increasing research interest described above, current climate model skill does not permit the necessary direct and detailed analysis of rerouting as a result of extreme-weather-causing extra fuel consumption, because parameters other than temperature still lack sufficient confidence. However, climate locations of existing flight trajectories are relatively easy to define as they are repetitious. Deviations from planned trajectories are apparent from the historical flight logs. Counting through the flight logs publicly available from 2000 to 2018, normalized by total traffic volume, shows no statistically robust time trend in flight track diversions and extensions. This lack of certainty is almost entirely due to the limited temporal extent of flight logs available at the time of writing this article. Hopefully, that will change in the future. Then, the impact on fuel costs of the increased weather-related impacts on aviation of climate change, revealed by the climate model projections, can be assessed.

Summary, conclusions, and future directions

In recent decade, the net constant top of atmosphere energy imbalance reached 1 W m^{-2} (Hu and Bates 2018). With the increased energy, the thermodynamic structure of the atmosphere has been substantially altered. There is an urgent need to go beyond the interpretation of the two most recent IPCC assessment reports (IPCC AR4, AR5), to address specific scientific and user issues in studies of climate change impacts on aviation. For example, previously the extent to which aviation fuel efficiency is affected by a more viscous atmosphere largely has been overlooked. In this study, warming climate impacts on net aviation fuel consumption are estimated using the CMIP5 climate model outputs (a 34-climate-model ensemble), based on a canonical fuel-burning equation, focusing on increased atmospheric viscosity at cruising altitudes. This is a highly complex topic and definitive conclusions are difficult to obtain

Downloaded from http://journals.ametsoc.org/bams/article-pdf/101/10/E1761/5013924/bamsd190239.pdf by guest on 24 November 2020

because different aspects of the problem respond differently to climate warming and there are many canceling mechanisms from simultaneous changes in temperature and air density. The stated research goal is achieved by 1) incorporating density into an aviation invariant and using the fact that air viscosity is a function only of temperature ("Methods, data sources, and processing" section); and 2) integrating an overarching fuel burning equation along realistic flight trajectories, with temperature-sensitive frictional drag parameterized according to the Sutherland equation. The five research imperatives investigated in the "Results and discussion" section are seamlessly unified under this primary fuel burning equation, representing the distinctive aspects of aviation fuel efficiency.

An along-route integration is made for all direct flights in the baseline year 2010 (Fig. 1), under current and future atmospheric conditions provided by 34 climate models, assuming the RCP8.5 strong emissions scenario. It is found that the percentage increase in fuel consumption from increased air viscosity is most sensitive to a warming climate; it is an order of magnitude higher than that due to reduced engine efficiency and the elevated tropopause. Because commercial airliners consume massive amounts of fossil fuel, the ~0.22% increase of total drag is equivalent to ~1.6×10^8 gallons of fuel annually, globally. The effects of frictional drag on increased fuel consumption, in addition being a dominant factor, also has the highest cross-climate model consistency, due to its direct relationship with air temperature, a primary output variable of the participating climate models. Consequently, extended to the fuel efficiency decrease, the intermodel spread is less than 5% of the mean value, over the entire period from 2000 to 2100. Compared with other possible effects on fuel efficiency arising from a warmer climate, the increased body drag is omnipresent and there are no easy pathways to circumvent it.

While the Bernoulli invariant and Sutherland relationship are immutable scientific laws that govern the consequences of a warming climate for civil aviation, aviation fuel efficiency also is a technological issue. In the case of fuel efficiency, technological advances, especially in the information technologies, may provide improved air traffic control to offset or even utilize the changes in airstreams, especially the jet streams and jet streaks, and to avoid severe weather events encountered during flight. Other possible consequences of the changing atmospheric structure in a warming climate, some of which are mentioned in the "Possible fuel efficiency impacts of other manifestations of climate warming" section, might become more pronounced in the future. The big data era offers opportunities to extend aviation research further in these directions.

It has been found in this study that climate warming likely has far-reaching consequences for civil aviation. Impact studies in this field still are in their embryonic stages, with few guidelines available for such research. After a robust analysis grounded in basic physical principles, it is convincing that reducing climate warming can trigger a benevolent loop for aviation, by increasing fuel efficiency and producing a smaller environmental footprint. This study is intended to assist far-ranging actions that attempt to reduce the impacts of a warming climate on civil aviation, rather than simply being an application of relatively elementary fluid dynamics. Finally, advances in fuel efficiency hopefully will ripple forward into feasible environmental benefits.

Acknowledgments. We thank J. Xu (Guangdong Marine University), D. Karoly (CSIRO), J. Zillman (BoM), and D. W. Fahey (NOAA/ESRL) for insightful discussion on aviation fuel efficiency in a warming climate. We also wish to acknowledge H. Thiemann for technical assistance in obtaining the IPCC AR5 data from the Deutsches Klimareshenzentrum (DKRZ) website. The work is jointly supported by Curtin University and School of Mathematical and Physical Sciences University of Technology Sydney. We thank L. Qi from BoM, Australia, for providing GrADS color palette schemes in Figs. 3 and 4.

Downloaded from http://journals.ametsoc.org/bams/article-pdf/101/10/E1761/5013924/bamsd190239.pdf by guest on 24 November 2020

References

Chapman, S., and T. Cowling, 1970: *The Mathematical Theory of Non-Uniform Gases*. 3rd ed. Cambridge University Press, 423 pp.

Chen, T., W. Rossow, and Y. Zhang, 2000: Radiative effects of cloud-type variations. *J. Climate*, **13**, 264–286, https://doi.org/10.1175/1520-0442(2000)013<0264:REOCTV>2.0.CO;2.

Coffel, E., and R. Horton, 2015: Climate change and the impact of extreme temperatures on aviation. *Wea. Climate Soc.*, **7**, 94–102, https://doi.org/10.1175/WCAS-D-14-00026.1.

Dee, D. P., and Coauthors, 2011: The ERA-Interim reanalysis: Configuration and performance of the data assimilation system. *Quart. J. Roy. Meteor. Soc.*, **137**, 553–597, https://doi.org/10.1002/qj.828.

Dessler, A., 2010: A determination of the cloud feedback from climate variations over the past decade. *Science*, **330**, 1523–1527, https://doi.org/10.1126/science.1192546.

Doyle, J. D., M. A. Shapiro, Q. Jiang, D. L. Bartels, 2005: Large-amplitude mountain wave breaking over Greenland. *J. Atmos. Sci.*, **62**, 3106–3126, https://doi.org/10.1175/JAS3528.1.

Gratton, G., A. Padhra, S. Rapsomanikis, and P. Williams, 2020: The impacts of climate change on Greek airports. *Climatic Change*, **160**, 219–231, https://doi.org/10.1007/s10584-019-02634-z.

Heymsfield, A., D. Baumgardner, P. DeMott, P. Forster, K. Gierens, and B. Kärcher, 2010: Contrail microphysics. *Bull. Amer. Meteor. Soc.*, **91**, 465–472, https://doi.org/10.1175/2009BAMS2839.1.

——, and Coauthors, 2017: Cirrus clouds. *Ice Formation and Evolution in Clouds and Precipitation: Measurement and Modeling Challenges*, *Meteor. Monogr.*, No. 58, Amer. Meteor. Soc., https://doi.org/10.1175/AMSMONOGRAPHS-D-16-0010.1.

Holman, J., 1980: *Thermodynamics*. McGraw-Hill, 217 pp.

Hu, A., and S. Bates, 2018: Internal climate variability and projected future regional steric and dynamic sea level rise. *Nat. Commun.*, **9**, 1068, https://doi.org/10.1038/s41467-018-03474-8.

ICAO, 2014: 2013-2028 global air navigation capacity and efficiency plan. International Civil Aviation Organization Tech. Doc. 9750, 137 pp., www.icao.int/meetings/anconf12/documents/Draft%20Doc%209750.GANP.en.pdf.

IPCC, 1999: *Aviation and the Global Atmosphere: A Summary for Policy Makers*. Cambridge University Press, 373 pp.

——, 2013: *Climate Change 2013: The Physical Science Basis*. Cambridge University Press, 1535 pp., https://doi.org/10.1017/CBO9781107415324.

Irvine, E. A., B. J. Hoskins, K. P. Shine, R. W. Lunnon, and C. Froemming, 2013: Characterizing North Atlantic weather patterns for climate-optimal aircraft routing. *Meteor. Appl.*, **20**, 80–93, https://doi.org/10.1002/met.1291.

Jenkins, A., and F. DiPaolo, 1956: Some physical properties of pure liquid ozone and ozone-oxygen mixtures. *J. Chem. Phys.*, **25**, 296–301, https://doi.org/10.1063/1.1742875.

Kalnay, E., and Coauthors, 1996: The NCEP/NCAR 40-Year Reanalysis Project. *Bull. Amer. Meteor. Soc.*, **77**, 437–471, https://doi.org/10.1175/1520-0477(1996)077<0437:TNYRP>2.0.CO;2.

Kim, J.-H., W. Chan, B. Sridhar, R. Sharman, P. Williams, and M. Strahan, 2016: Impact of the North Atlantic Oscillation on transatlantic flight routes and clear-air turbulence. *J. Appl. Meteor. Climatol.*, **55**, 763–771, https://doi.org/10.1175/JAMC-D-15-0261.1.

Kobayashi, S., and Coauthors, 2015: The JRA-55 Reanalysis: General specifications and basic characteristics. *J. Meteor. Soc. Japan*, **93**, 5–48, https://doi.org/10.2151/JMSJ.2015-001.

Lee, D., and D. Fahey, 2016: Aviation and climate change: A scientific perspective. *Carbon Climate Law Rev.*, **10**, 97–104.

——, ——, P. Forster, P. Newton, R. Wit, L. Lim, B. Owen, and R. Sausen, 2009: Aviation and global climate change in the 21st century. *Atmos. Environ.*, **43**, 3520–3537, https://doi.org/10.1016/j.atmosenv.2009.04.024.

Lee, S., P. Williams, and T. Frame, 2019: Increased shear in the North Atlantic upper-level jet stream over the past four decades. *Nature*, **572**, 639–642, https://doi.org/10.1038/s41586-019-1465-z.

Lewis, S., and D. Karoly, 2015: Are estimates of anthropogenic and natural influences on Australia's extreme 2010–2012 rainfall model-dependent? *Climate Dyn.*, **45**, 679–695, https://doi.org/10.1007/s00382-014-2283-5.

Liou, K., 1986: Influence of cirrus clouds on weather and climate processes: A global perspective. *Mon. Wea. Rev.*, **114**, 1167–1199, https://doi.org/10.1175/1520-0493(1986)114<1167:IOCCOW>2.0.CO;2.

Lorenz, D., and E. DeWeaver, 2007: Tropopause height and zonal wind response to global warming in the IPCC scenario integrations. *J. Geophys. Res.*, **112**, D10119, https://doi.org/10.1029/2006JD008087.

Mattingly, J., W. Heiser, and D. Pratt, 2002: *Aircraft Engine Design*. 2nd ed. American Institute of Aeronautics and Astronautics Inc., 719 pp.

Reichler, T., D. Martin, and R. Sausen, 2003: Determining the tropopause height from gridded data. *Geophys. Res. Lett.*, **30**, 2042, https://doi.org/10.1029/2003GL018240.

Ren, D., 2010: Effects of global warming on wind energy availability. *J. Renewable Sustainable Energy*, **2**, 052301, https://doi.org/10.1063/1.3486072.

——, and L. M. Leslie, 2015: Changes in tropical cyclone activity over northwest Western Australia in the past 50 years and a view of the future 50 years. *Earth Interact.*, **19**, https://doi.org/10.1175/EI-D-14-0006.1.

——, and ——, 2019a: Impacts of climate warming on aviation fuel consumption. *J. Appl. Meteor. Climatol.*, **58**, 1593–1602, https://doi.org/10.1175/JAMC-D-19-0005.1.

——, and ——, 2019b: Climate warming and effects on civil aviation. *Environmental Impact of Aviation and Sustainable Solutions*, R. K. Agarwal, Ed., IntechOpen, https://doi.org/10.5772/intechopen.86871.

——, R. Fu, L. M. Leslie, J. Chen, C. R. Wilson, and D. J. Karoly, 2011: The Greenland ice sheet response to transient climate change. *J. Climate*, **24**, 3469–3483, https://doi.org/10.1175/2011JCLI3708.1.

——, R. Dickinson, R. Fu, J. Bornman, W. Guo, S. Yang, and L. Leslie, 2018: The impacts of climate warming on maximum aviation payloads. *Climate Dyn.*, **52**, 1711–1721, https://doi.org/10.1007/S00382-018-4399-5.

Santer, B., and Coauthors, 2003: Behavior of tropopause height and atmospheric temperature in models, reanalyses, and observations: Decadal changes. *J. Geophys. Res.*, **108**, 4002, https://doi.org/10.1029/2002JD002258.

Sausen, R., and Coauthors, 2005: Aviation radiative forcing in 2000: An update on IPCC (1999). *Meteor. Z.*, **14**, 555–561, https://doi.org/10.1127/0941-2948/2005/0049.

Sharman, R., C. Tibaldi, C. Weiner, and J. Wolff, 2006: An integrated approach to mid- and upper-level turbulence forecasting. *Wea. Forecasting*, **21**, 268–287, https://doi.org/10.1175/WAF924.1.

——, B. Trier, T. Lane, and J. Doyle, 2012a: Sources and dynamics of turbulence in the upper troposphere and lower stratosphere: A review. *Geophys. Res. Lett.*, **39**, L12803, https://doi.org/10.1029/2012GL051996.

——, J. Doyle, and M. Shapiro, 2012b: An investigation of a commercial aircraft encounter with severe clear-air turbulence over western Greenland. *J. Appl. Meteor. Climatol.*, **51**, 42–53, https://doi.org/10.1175/JAMC-D-11-044.1.

Storer, L., P. Williams, and M. Joshi, 2017: Global response of clear-air turbulence to climate change. *Geophys. Res. Lett.*, **44**, 9976–9984, https://doi.org/10.1002/2017GL074618.

——, ——, and P. Gill, 2018: Aviation turbulence: Dynamics, forecasting, and response to climate change. *Pure Appl. Geophys.*, **176**, 2081–2095, https://doi.org/10.1007/S00024-018-1822-0.

Suarez, M. J., and Coauthors, 2008: The GEOS-5 Data Assimilation System—Documentation of versions 5.0.1, 5.1.0, and 5.2.0. NASA Tech. Memo. NASA/TM-2008-104606, Vol. 27, 101 pp., https://gmao.gsfc.nasa.gov/pubs/docs/Rienecker369.pdf.

Taylor, K., R. Stouffer, and G. Meehl, 2012: An overview of CMIP5 and the experiment design. *Bull. Amer. Meteor. Soc.*, **93**, 485–498, https://doi.org/10.1175/BAMS-D-11-00094.1.

Tennekes, H., 2009: *The Simple Science of Flight*. MIT Press, 216 pp.

Downloaded from http://journals.ametsoc.org/bams/article-pdf/101/10/E1761/5013924/bamsd190239.pdf by guest on 24 November 2020

Turner, M., I. MacLeod, and A. Rothberg, 1989: Effects of temperature and composition on the viscosity of respiratory gases. *J. Appl. Physiol.*, **67**, 472–477, https://doi.org/10.1152/jappl.1989.67.1.472.

Vallis, G., P. Zurita-Gotor, C. Cairns, and J. Kidston, 2015: Response of the large-scale structure of the atmosphere to global warming. *Quart. J. Roy. Meteor. Soc.*, **141**, 1479–1501, https://doi.org/10.1002/qj.2456.

Voigt, C., and Coauthors, 2017: ML-CIRRUS: The airborne experiment on natural cirrus and contrail cirrus with the high-altitude long-range research aircraft HALO. *Bull. Amer. Meteor. Soc.*, **98**, 271–288, https://doi.org/10.1175/BAMS-D-15-00213.1.

Wallace, J., and P. Hobbs, 1977: *Atmospheric Science: An Introductory Survey*. Academic Press, 467 pp.

——, C. Smith, and C. Bretherton, 1992: Singular value decomposition of wintertime sea surface temperature and 500-mb height anomalies. *J. Climate*, **5**, 561–576, https://doi.org/10.1175/1520-0442(1992)005<0561:SVDOWS>2.0.CO;2.

Williams, P., 2016: Transatlantic flight times and climate change. *Environ. Res. Lett.*, **11**, 024008, https://doi.org/10.1088/1748-9326/11/2/024008.

——, 2017: Increased light, moderate, and severe clear-air turbulence in response to climate change. *Adv. Atmos. Sci.*, **34**, 576–586, https://doi.org/10.1007/s00376-017-6268-2.

——, and M. Joshi, 2013: Intensification of winter transatlantic aviation turbulence in response to climate change. *Nat. Climate Change*, **3**, 644–648, https://doi.org/10.1038/nclimate1866.

WMO, 2018: Scientific assessment of ozone depletion: 2018. Global Ozone Research and Monitoring Project Rep. 58, 588 pp.

Zillman, J., 1997: Atmospheric science and public policy. *Science*, **276**, 1084–1086, https://doi.org/10.1126/science.276.5315.1084.

Downloaded from http://journals.ametsoc.org/bams/article-pdf/101/10/E1761/5013924/bamsd190239.pdf by guest on 24 November 2020

Copyright of Bulletin of the American Meteorological Society is the property of American Meteorological Society and its content may not be copied or emailed to multiple sites or posted to a listserv without the copyright holder's express written permission. However, users may print, download, or email articles for individual use.